

A NEW DEFORMATION FAMILY OF SCHWARZ' D SURFACE

HAO CHEN AND MATTHIAS WEBER

ABSTRACT. We prove the existence of a new 2-parameter family $\mathfrak{o}\Delta$ of embedded triply periodic minimal surfaces of genus 3. The new surfaces share many properties with classical orthorhombic deformations of Schwarz' D surface, but also exotic in many ways. In particular, they do not belong to Meeks' 5-dimensional family. Nevertheless, $\mathfrak{o}\Delta$ meets classical deformations in a 1-parameter family on its boundary.

1. INTRODUCTION

In the past three decades, the classification of complete, embedded minimal surface of finite topology in Euclidean space forms has largely been accomplished for the smallest reasonable genus ([MPR98, LHM01, PRT05, MR05, PT07]). A notable exception has been the classification of embedded triply periodic minimal surfaces (TPMS) of genus 3. A main difficulty is that, in addition to the quite explicit 5-dimensional family discovered by Meeks [Mee90], there are more elusive surfaces not in this family.

We will exhibit a 1-parameter family of embedded TPMS of genus 3 in the junction of the Meeks family and non-Meeks surfaces. More specifically, these surfaces are *bifurcation instances* in the sense that, with the same deformation of their lattices, they may deform either within a classical 2-parameter Meeks family, or into a new 2-parameter non-Meeks family. Existence of the latter is the focus of this paper.

In fact, all these surfaces are orthorhombic deformations of Schwarz' D surface. Hence we begin with a description of the classical orthorhombic deformations of D.

Date: May 27, 2022.

2010 *Mathematics Subject Classification.* Primary 53A10.

Key words and phrases. Triply periodic minimal surfaces.

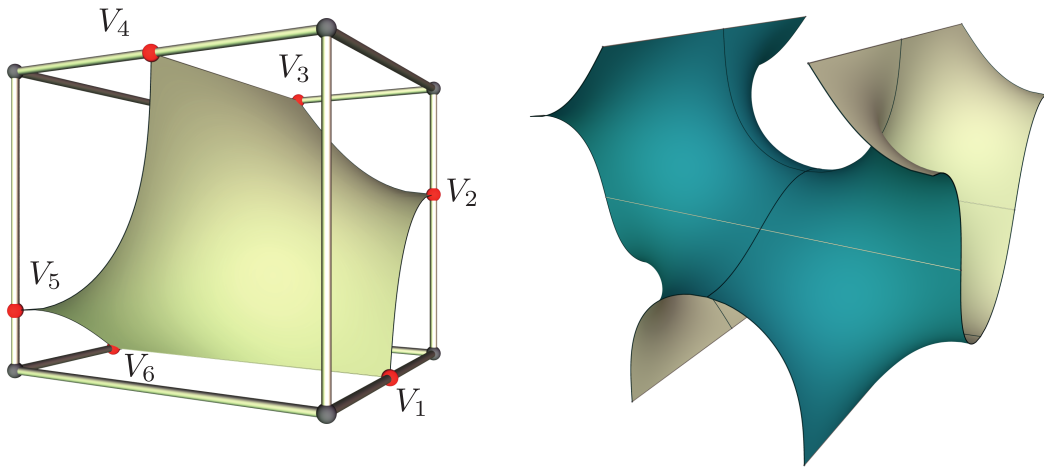


FIGURE 1.1. Fundamental Piece and Translational Fundamental Piece

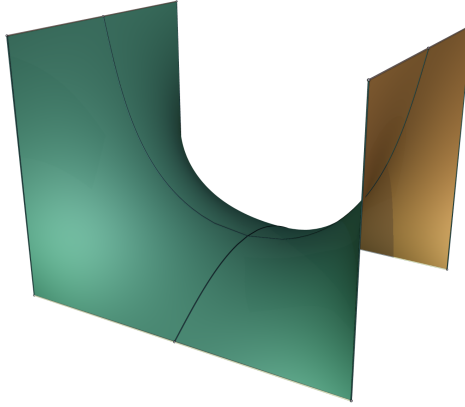


FIGURE 1.2. Plateau construction of oD surfaces

Consider an embedded minimal surface S inside an axis parallel box $[-A, A] \times [-B, B] \times [0, 1]$ that solves the following partially free boundary problem: S satisfies free boundary condition on the vertical planes $x = \pm A$ and $y = \pm B$, and fixed (Plateau) boundary condition on the horizontal segments $\{(x, 0, 0) \mid -A \leq x \leq A\}$ and $\{(0, y, 1) \mid -B \leq y \leq B\}$, and the intersection of ∂S with each face of the box has at most one component. S is therefore an right-angled embedded minimal hexagon. See Figure 1.1 (left) for an example.

Because the two horizontal segments are in the middle of the top and bottom faces of the box, rotations about them and reflections in the lateral faces of the box extend S to an embedded TPMS \tilde{S} . More specifically, \tilde{S} is invariant under the lattice Λ spanned by $(2A, 0, 0)$, $(0, 2B, 0)$ and $(A, B, 2)$. In the 3-torus \mathbb{R}^3 , \tilde{S}/Λ is a compact surface of genus 3. In Figure 1.1 (right) we show a translational fundamental domain of \tilde{S} presented nicely in a box. It consists of 8 copies of S .

Remark 1.1. For crystallographers, the orthorhombic lattice spanned by $(2A, 0, 0)$, $(0, 2B, 0)$ and $(0, 0, 4)$ is more convenient. This is responsible for the letter “o” in our naming.

We use \mathcal{D} to denote the set of all TPMS obtained in this way.

A well-known family of surfaces in \mathcal{D} is the tD family of H. A. Schwarz, which is a tetragonal deformation family of his famous D surface. They are obtained as described above with $A = B$ and S containing the vertical segment $\{(0, 0, z) \mid 0 \leq z \leq 1\}$. The same construction also applies when $A \neq B$, yielding an orthorhombic deformation of Schwarz’ D surface, known as oDb in the literature to distinguish from another orthorhombic deformation family oDa; see [FK89, FH92]. In this paper, we simply use oD in place of oDb.

An alternative (better known) construction of an oD surface starts with a box of the same dimensions and then solves the Plateau problem for a polygonal contour running along edges of the box, as shown in Figure 1.2. The Plateau solution is unique and therefore shares the symmetries of the contour. In particular, it has reflectional symmetries by vertical planes. To relate with the previous construction, just divide the minimal surface into quarts by cutting along these planes, then extend one of the quarts by rotating it about its vertical edge.

The main result of this paper is to confirm the existence of another 2-parameter family in \mathcal{D} .

Theorem 1.2. *There exists a second 2-parameter family $\text{o}\Delta$ in \mathcal{D} , lacking the vertical straight line of the oD surfaces.*

Usually, at least for low genus, one does not expect less symmetric minimal surfaces when more symmetric ones exist. The second author confesses his complete bafflement and initial disbelief when the first author provided him with evidence of $\text{o}\Delta$. In Figure 1.3 we compare oD and $\text{o}\Delta$ surfaces with the same lattice (the surfaces in this figure actually have tetragonal lattices, hence belong to tD and t Δ subfamilies that we will discuss later.)

The $\text{o}\Delta$ family is not merely a surprise. Its significance is revealed in the following proposition.

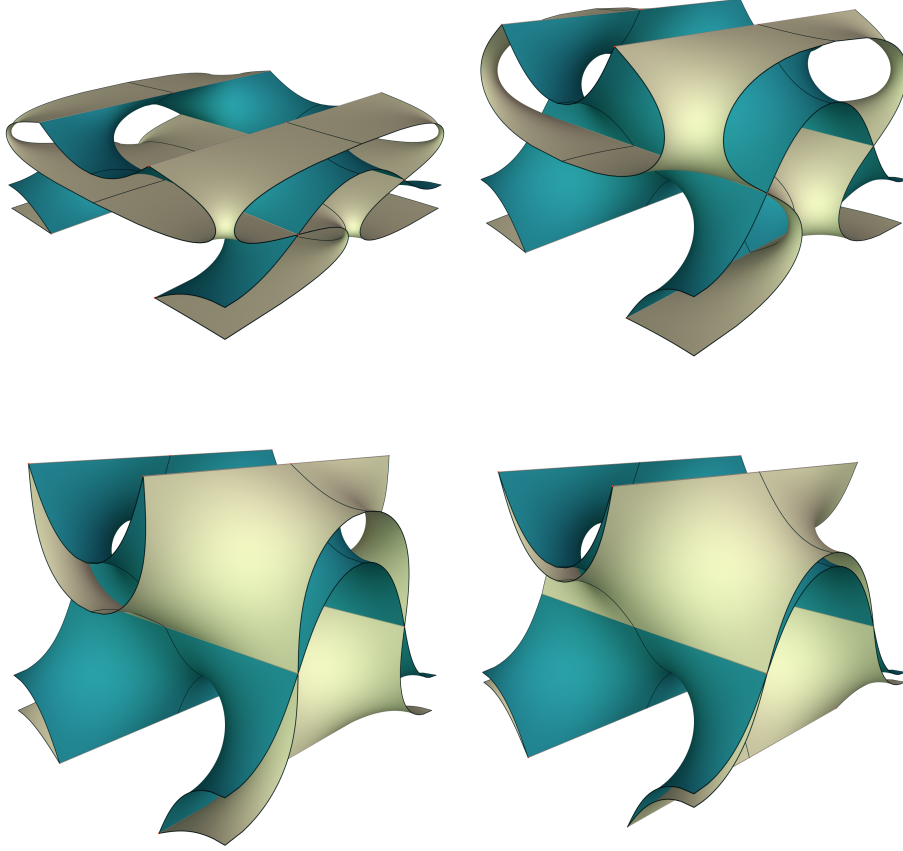


FIGURE 1.3. Comparison of oD (dark) and o Δ (bright) surfaces with the same lattice. These surfaces actually belong to the tD and t Δ subfamily.

Proposition 1.3. *The surfaces in o Δ do not belong to the Meeks family. That is, the branched values of the Gauss map of an o Δ surface do not form four antipodal pairs. In fact, the only Meeks surfaces in \mathcal{D} are the oD surface. However, the closure $\overline{o\Delta}$ intersects oD in a 1-parameter family of TPMS.*

We now provide some context for the proposition.

For the purpose of this paper, a TPMS is a complete, embedded minimal surface $\tilde{\Sigma}$ in Euclidean space \mathbb{R}^3 invariant under a lattice Λ of Euclidean translate. The quotient $\Sigma = \tilde{\Sigma}/\Lambda$ then is a compact Riemann surface in the 3-torus \mathbb{R}^3/Λ . The lowest possible genus for a non-trivial TPMS is 3. In this case, the Gauss map of Σ has degree 2, and the surface is therefore necessarily hyperelliptic.

The first examples of TPMS were given by H. A. Schwarz [Sch90] around 1867, with explicit Weierstrass data for very symmetric cases. Schwarz understood that the eight branched values of the Gauss map play a crucial role. More generally, W. Meeks III [Mee90] explicitly constructed a family \mathcal{M} of TPMS of genus 3. He showed that if eight points on the sphere come in four antipodal pairs, then they are the branched values of the Gauss map for two conjugate TPMS of genus 3. The Meeks family \mathcal{M} , considered up to congruence and dilation, is a connected, smooth, (real) 5-dimensional manifold, and includes almost all previously known examples.

Famous exceptions are the H surfaces of Schwarz, for which the branched values are placed at the north pole, the south pole, and the vertices of a prism over an equilateral triangle inside the

sphere; and the Gyroid of A. Schoen [Sch70], whose Gauss map has the same branched values as those of Schwarz' P and D surfaces, but does not belong to the Meeks family. We use \mathcal{N} to denote the complement of \mathcal{M} in the set of all TPMS of genus 3. Since then, more examples in \mathcal{N} have been found, either as isolated examples or as 1-parameter families, and some of them only numerically [FHL93, FH99, Wey06, Wey08]. Our 2-parameter family $\text{o}\Delta$ is therefore an important step towards the understanding of non-Meeks TPMS of genus 3.

Meeks' result is extended into the following rigidity statement: In the neighborhood of a non-degenerate TPMS, there is a bijection between TPMS and lattices in \mathbb{R}^3 ; see [KPS14] for instance. Hence up to congruence and dilation, a non-degenerate TPMS belongs (locally) to a 5-parameter family. Besides that, very little is known about the structure of \mathcal{N} . We would like to conjecture that \mathcal{N} is, like \mathcal{M} , connected and smooth, but none of these is known.

There is evidence [FHL93, FH99, Wey06, Wey08] that \mathcal{M} and the closure $\overline{\mathcal{N}}$ have non-empty intersection. Proposition 1.3 provides the first concrete example of such intersection in the form of a 1-dimensional family of TPMS. This is of considerable importance for stability questions of TPMS.

A TPMS of genus 3 is called a *bifurcation instance* if there are non-congruent deformations (bifurcation branches) of the TPMS with the same deformation of the lattice. Koiso, Piccione and Shoda [KPS14] identified isolated *bifurcation instances* among classical deformations of TPMS; see also [ES14, ES18]. They found bifurcation branches for most of these bifurcation instances. But for three “exotic” bifurcation instances, they only suggested that a bifurcation branch from them would not be a “classical” TPMS.

The intersection $\text{o}\Delta \cap \text{oD}$ is a 1-parameter family of bifurcation instances. In particular, a 1-parameter subfamily of $\text{o}\Delta$, which we call $\text{t}\Delta$, has the same tetragonal lattices as the tD family. The intersection $\text{t}\Delta \cap \text{tD}$ contains a single TPMS, denoted by tD^* , which turns out to be one of the exotic bifurcation instances in [KPS14]. We also find a bifurcation branch $\text{t}\Pi$ from the conjugate of tD^* , another exotic bifurcation instance in Schwarz' tP family. But $\text{t}\Pi$ is not the focus of this paper, since it is nothing but a classical oPa deformation [FK89, FH92].

For sufficiently large A and B , the existence of $\text{o}\Delta$ surfaces is implied by results of Traizet [Tra08], who constructed TPMS by opening catenoidal nodes among 2-tori. The positions of the nodes have to satisfy a balance condition, formulated in terms of elliptic functions, and a non-degeneracy condition. The Traizet limit of $\text{o}\Delta$ was noted by the first author in an earlier experimental work [Che18]. He used Brakke's Surface Evolver [Bra92] to numerically deform the TPMS from near the Traizet limit up to Schwarz' tD family, and obtained the first images of $\text{t}\Delta$. In particular, he observed that $\text{t}\Delta$ eventually intersects tD , but Surface Evolver fails to converge near the intersection. This failure can now be explained by numeric bifurcation.

Our paper is organized as follows:

In Section 2, we describe the Weierstrass data for surfaces in \mathcal{D} and formulate the period problem, depending on three real positive parameters a, b and t . The case $a = b$ corresponds to the oD surfaces, where the period problem is automatically solved. Away from $a = b$, the period problem becomes 1-dimensional but is rather complicated.

In Section 3 we show that, if $a \neq b$, the branched values of the Gauss map can *not* be antipodal. This proves that $\mathcal{D} \cap \mathcal{M} = \text{oD}$, and that any solution with $a \neq b$ (namely $\text{o}\Delta$) lies in \mathcal{N} .

Section 4 is dedicated to the existence proof of $\text{o}\Delta$. We show that for any choice of $a \neq b$, there is a value of t that solves the period problem. This is accomplished through a careful asymptotic analysis of the period integrals. We also conjecture the uniqueness of t based on numerical experiments.

To prove that $\text{oD} \subset \mathcal{M}$ and the closure of $\text{o}\Delta \subset \mathcal{N}$ have a non-empty intersection, we consider in Section 5 a modified period problem that eliminates the trivial solutions coming from oD . It turns out that this period problem can be solved explicitly in terms of elliptic integrals.

In section 6 we consider the surfaces with tetragonal lattices. They are \mathcal{D} surfaces whose parameters satisfy $ab = t$. In this case, we obtain two 1-parameter families of surfaces: $\text{tD} \subset \text{oD}$ containing Schwarz' D surface, and $\text{t}\Delta \subset \text{o}\Delta$. The intersection $\overline{\text{t}\Delta} \cap \text{tD}$ contains a single TPMS

tD^* . As the existence of $t\Delta$ does not follow from Section 4, we give an independent proof for this case using an extremal length argument.

Acknowledgements. The first author thanks his newborn daughter for keeping him awake through the nights, which helped noticing the $t\Delta$ family.

The second author thanks his teenage daughter for keeping him sleepless as well, thus providing time to work on this paper.

2. WEIERSTRASS DATA AND PERIOD PROBLEM

We parameterise a surface in \mathcal{D} with a Weierstrass representation defined on the upper half plane such that the real axis is mapped to the boundary of the hexagon S . Let the vertices of S be labeled by V_1, V_2, \dots, V_6 as in Figure 1.1 (left). Denote the preimage of V_k by $v_k \in \mathbb{R}$, and assume that $v_1 < v_2 < \dots < v_6$.

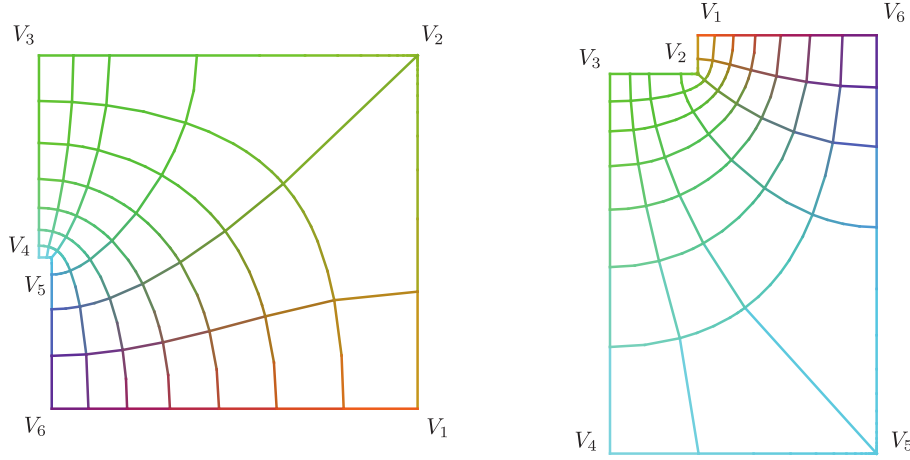


FIGURE 2.1. Images of a fundamental piece under Φ_1 and Φ_2 .

Given a \mathcal{D} surface, denote by dh its height differential and by G its Gauss map. Let $\phi_1 := dh \cdot G$ and $\phi_2 := dh/G$. The assumed boundary symmetries of the surface imply that $\Phi_j : z \mapsto \int^z \phi_j$ ($j = 1$ or 2) map the upper half plane to “right angled” Euclidean hexagons. The interior angle is 270° at $\Phi_1(v_5)$ and $\Phi_2(v_2)$. Indeed, the Gauss map is vertical at V_2 and V_5 , hence v_2 and v_5 are respectively the pole and the zero of G . Interior angles at all other vertices are 90° ; see Figure 2.1.

Such maps are given by Schwarz-Christoffel maps. More specifically, we have

$$\begin{aligned} \phi_1 &:= \rho(z - v_1)^{-1/2}(z - v_2)^{-1/2}(z - v_3)^{-1/2}(z - v_4)^{-1/2}(z - v_5)^{+1/2}(z - v_6)^{-1/2} dz, \\ \phi_2 &:= -\frac{1}{\rho}(z - v_1)^{-1/2}(z - v_2)^{+1/2}(z - v_3)^{-1/2}(z - v_4)^{-1/2}(z - v_5)^{-1/2}(z - v_6)^{-1/2} dz, \\ dh &:= -i(z - v_1)^{-1/2} \times (z - v_3)^{-1/2}(z - v_4)^{-1/2} \times (z - v_6)^{-1/2} dz. \end{aligned}$$

Here, the real positive Lopéz-Ros factor ρ determines scaling of the image domains. The Gauss map is $G := i\rho(z - v_2)^{-1/2}(z - v_5)^{+1/2}$.

Proposition 2.1. *Up to congruence and dilation, the image of the upper half plane under the map*

$$(2.1) \quad z \mapsto \operatorname{Re} \int^z (\omega_1, \omega_2, \omega_3) = \operatorname{Re} \int^z \left(\frac{1}{2}(\phi_2 - \phi_1), \frac{i}{2}(\phi_2 + \phi_1), dh \right)$$

is almost the fundamental hexagon of a \mathcal{D} surface in the following sense: The intervals v_1v_2 , v_2v_3 , v_4v_5 and v_5v_6 are mapped to planar symmetry curves in the lateral faces of an axis parallel box. The intervals v_6v_1 and v_3v_4 are mapped, respectively, to straight segments parallel to the x and y axis, but not necessarily in the middle, in the bottom and top faces of the box.

Proof. Note that the integrand in ϕ_1 (resp. ϕ_2) is real positive (resp. negative) for $z > v_6$. This implies that the image of the segment v_6v_1 under the Schwarz-Christoffel map Φ_1 (resp. Φ_2) is horizontal rightward (resp. leftward), as in Figure 2.1.

The Schwarz-Christoffel maps Φ_j and $z \mapsto \int^z dh$ can be continued by reflection across any edge to the lower half plane, inducing symmetries of the minimal surface. We now determine what kind of symmetry is induced on each edge.

For that, we only carry out a detailed analysis on the edge v_6v_1 . The integrands in both ϕ_j are real on v_6v_1 , hence their continuations across this edge are given by $\overline{\phi_j(\bar{z})}$. Meanwhile, the integrand in dh is imaginary on v_6v_1 , so its continuation is given by $-\overline{dh(\bar{z})}$. Therefore, after crossing v_6v_1 , $\text{Re } \omega_1$ remains unchanged while $\text{Re } \omega_2$ and $\text{Re } \omega_3$ change sign. This means that the surface is extended by a rotation about a straight line parallel to the x -axis.

Similar analysis on the other edges then prove that the image of the upper half plane under (2.1) has the claimed boundary curves. Note that the surface obtained is free of singularities. Indeed, the metrics is regular away from v_k , and the exponents at v_k guarantee a smooth extension. \square

We now study the condition for the two horizontal segments to lie in the middle of the top and the bottom faces of the box. To this end, we introduce notations for the edge lengths of the Euclidean hexagons

$$I_k := \left| \int_{v_k}^{v_{k+1}} \phi_1 \right|, \quad J_k := \left| \int_{v_k}^{v_{k+1}} \phi_2 \right|$$

for $1 \leq k \leq 5$. These are positive real numbers that depend analytically on the parameters v_1, \dots, v_6 and ρ .

Proposition 2.2. *The image of the upper half plane under the Weierstrass representation (2.1) is the fundamental hexagon of a surface in \mathcal{D} if and only if the following period conditions are satisfied:*

$$(2.2) \quad \begin{aligned} I_1 + I_5 &= J_1 + J_5 \\ I_2 + I_4 &= J_2 + J_4 \end{aligned}$$

Proof. The bottom segment V_6V_1 lies in the middle of the bottom face if and only if

$$\text{Re} \int_{v_1}^{v_2} \omega_2 = \text{Re} \int_{v_5}^{v_6} \omega_2.$$

This is equivalent to

$$\text{Im} \int_{v_1}^{v_2} (\phi_2 + \phi_1) = \text{Im} \int_{v_5}^{v_6} (\phi_2 + \phi_1).$$

Observe on v_1v_2 that the integrand in ϕ_1 (resp. ϕ_2) is positive (resp. negative) imaginary, and on v_5v_6 that the integrand in ϕ_1 (resp. ϕ_2) is negative (resp. positive) imaginary. So the equation above can be written as

$$I_1 - J_1 = J_5 - I_5,$$

which proves the first period condition. The second follows analogously. \square

We can eliminate ρ by taking the quotient of the two equations, therefore:

Corollary 2.3. *If*

$$Q_I := \frac{I_1 + I_5}{I_2 + I_4} = \frac{J_1 + J_5}{J_2 + J_4} =: Q_J$$

or, equivalently, if

$$(2.3) \quad Q := Q_I - Q_J = \frac{I_1 + I_5}{I_2 + I_4} - \frac{J_1 + J_5}{J_2 + J_4} = 0$$

for some choice of v_1, \dots, v_6 , then $\rho \in \mathbb{R}_{>0}$ can be uniquely adjusted so that the period conditions (2.2) are satisfied.

Thus we have expressed the period condition as a single equation $Q = 0$, where Q depends on six parameters v_1, \dots, v_6 . The number of parameters can be reduced to three after a normalization by Möbius transformations. More specifically, we can assume

$$v_1 = -t, v_2 = -a, v_3 = -1, v_4 = 1, v_5 = b, v_6 = t$$

with $-t < -a < -1 < 1 < b < t$. We also assume that $a \leq b$. If it is not the case, we may simply switch a and b ; this only exchanges I_k and J_{6-k} , $1 \leq k \leq 5$, up to the scaling ρ , hence leaves Q invariant.

We note two special cases.

If $a = b$, the period conditions (2.2) are satisfied automatically with $\rho = 1$. In this case, the involution $z \mapsto -\bar{z}$ induces an order-2 rotation of the surface in a vertical axis. This can be seen by noting that ω_1 and ω_2 change sign but ω_3 keeps sign under the involution. Indeed, on the imaginary axis (fixed by the involution), ϕ_1 and ϕ_2 are conjugate and dh is real. Hence the positive imaginary axis is mapped by the Weierstrass representation (2.1) to the vertical straight segment between the middle points of V_3V_4 and of V_6V_1 , which serves as the axis of the order-2 rotation. This shows that the surface is in oD.

If $ab = t$, the involution $z \mapsto -t/z$ induces an order-2 rotation of the surface that exchanges V_k with V_{k+3} , $1 \leq k \leq 3$. In particular, the segments V_6V_1 and V_3V_4 must have the same length, implying that the bounding box has a square base. The unique fixed point of the involution, namely $i\sqrt{t}$, is mapped to the fixed point of the rotation. We will consider this case in detail in Section 6.

3. BRANCHED VALUES OF THE GAUSS MAP

To locate the branched points of the Gauss map, we use the following simple observation:

Lemma 3.1. *At every orthogonal intersection of a planar symmetry curve and a straight line on a minimal surface, the Gauss map has a branched point.*

Proof. At points on the straight line that are symmetric with respect to the symmetry plane, the Gauss map takes the same value. Hence it cannot be single valued in a neighborhood of the intersection point. \square

We now show

Theorem 3.2. *The branched points of the Gauss map of a surface in \mathcal{D} are antipodal if and only if $a = b$.*

Proof. By the Lemma, the Gauss map has branched points at V_1, V_3, V_4 and V_6 . On a translational fundamental domain, each of these points occurs twice, giving eight branched points as expected.

Recall that the Gauss map is given by

$$G(z) = i\rho(z+a)^{-1/2}(z-b)^{+1/2}.$$

We then compute the branched values in \mathbb{S}^2 explicitly by the stereographic projection

$$\sigma(z) = \frac{1}{|z|^2 + 1} (2 \operatorname{Re}(z), 2 \operatorname{Im}(z), |z|^2 - 1),$$

and obtain

$$\begin{aligned} \sigma(\pm G(+1)) &= \frac{(\mp 2\rho\sqrt{(a+1)(b-1)}, 0, \rho^2(b-1) - (a+1))}{\rho^2(b-1) + (a+1)} \\ \sigma(\pm G(-1)) &= \frac{(\mp 2\rho\sqrt{(a-1)(b+1)}, 0, \rho^2(b+1) - (a-1))}{\rho^2(b+1) + (a-1)} \\ \sigma(\pm G(+t)) &= \frac{(0, \pm 2\rho\sqrt{(t+a)(t-b)}, \rho^2(t-b) - (t+a))}{\rho^2(t-b) + (t+a)} \\ \sigma(\pm G(-t)) &= \frac{(0, \pm 2\rho\sqrt{(t-a)(t+b)}, \rho^2(t+b) - (t-a))}{\rho^2(t+b) + (t-a)} \end{aligned}$$

We see that they lie in the coordinate planes $x = 0$ and $y = 0$, respectively, which helps matching them in possible antipodal pairs.

Recall that $-t < -a < -1 < 1 < b < t$. Assume that the branched values do occur in antipodal pairs and, for the sake of contradiction, that $a \neq b$. First note that $\sigma(G(+1))$ and $\sigma(-G(+1))$ cannot be antipodal. Otherwise, their last coordinates must be 0, forcing $b = 1$ and $a = -1 < 0$ which violates our assumption. By the same argument, $\sigma(G(-1))$ and $\sigma(-G(-1))$ are not antipodal, neither. Thus the only possibility is that $\pm G(-1)$ and $\pm G(+1)$ are antipodal, with two possible choices of signs. Either choice implies that the last coordinates have opposite signs, which reduces to

$$\rho^4 = \frac{a^2 - 1}{b^2 - 1}.$$

The same analysis on $\sigma(\pm G(\pm a))$ leads to

$$\rho^4 = \frac{t^2 - a^2}{t^2 - b^2}.$$

Combining the two equations for ρ^4 shows, after a brief computation, that either $t = 0$ or $a = b$. The contradiction with our assumptions proves the “only if”.

For the “if” part, assume that $a = b$. Then we find the branched points become antipodal (only) with $\rho = 1$. More specifically, we have

$$\begin{aligned}\sigma(\pm G(+1)) &= \left(\mp \frac{\sqrt{a^2 - 1}}{a}, 0, -\frac{1}{a} \right) \\ \sigma(\pm G(-1)) &= \left(\mp \frac{\sqrt{a^2 - 1}}{a}, 0, +\frac{1}{a} \right) \\ \sigma(\pm G(+t)) &= \left(0, \pm \frac{\sqrt{t^2 - a^2}}{t}, -\frac{a}{t} \right) \\ \sigma(\pm G(-t)) &= \left(0, \pm \frac{\sqrt{t^2 - a^2}}{t}, +\frac{a}{t} \right)\end{aligned}$$

Geometrically, these points on the unit sphere are vertices of two axis parallel rectangles in the planes $x = 0$ and $y = 0$, respectively. Remarkably, an image of two such rectangles already appears in Figure 44 of the *Nachtrag* of Schwarz’ paper “Bestimmung einer speciellen Minimalfläche” from 1867. \square

We note that in the case $a = b$ the branched values lie at the vertices of a cube if and only of $a^2 = b^2 = t = 2$. This is the case of the classical D surface of Schwarz.

4. EXISTENCE OF NON-TRIVIAL SOLUTIONS

Recall that $1 < a \leq b < t$, and the periodic condition (2.3) as we copy below

$$Q(a, b; t) = \frac{I_1 + I_5}{I_2 + I_4} - \frac{J_1 + J_5}{J_2 + J_4} = 0.$$

The quantity Q is our focus in the remaining of this paper. From now on, we will ignore the Lopéz-Ros factor ρ in our calculations, since Q is independent of this factor.

We now prove the main theorem of this paper.

Theorem 4.1. *If $a = b$, the period condition (2.3) is solved for any choice of t .*

If $a < b$, then there exists a value of t that solves the period condition (2.3).

The case $a = b$ has been discussed in Section 2. The case $a < b$ follows from the continuity of Q in t , and the following proposition.

Proposition 4.2. *If $1 < a < b < t$ then*

$$(4.1) \quad \lim_{t \rightarrow b+} Q(a, b; t) > 0,$$

$$(4.2) \quad \lim_{t \rightarrow +\infty} Q(a, b; t) = -\infty.$$

The remainder of this section is devoted to the proof of this proposition.

We begin by analyzing the limit $t \rightarrow b+$.

Proof of (4.1). We can evaluate the period integrals explicitly. Recall that, if $p < q$, we have

$$\int_p^q \sqrt{\frac{1}{(q-z)(z-p)}} dz = \pi, \quad \int_p^q \sqrt{\frac{z-p}{q-z}} dz = \frac{q-p}{2} \pi.$$

Therefore the integrals

$$\begin{aligned} \lim_{t \rightarrow b+} I_1(a, b; t) &= C \int_a^t \sqrt{\frac{1}{(t-z)(z-a)}} dz, & \lim_{t \rightarrow b+} J_1(a, b; t) &= C \int_a^t \sqrt{\frac{z-a}{t-z}} dz, \\ \lim_{t \rightarrow b+} I_2(a, b; t) &= C \int_1^a \sqrt{\frac{1}{(a-z)(z-1)}} dz, & \lim_{t \rightarrow b+} J_2(a, b; t) &= C \int_1^a \sqrt{\frac{z-1}{a-z}} dz \end{aligned}$$

are all bounded and non-zero. Here C can denote any bounded positive number. Moreover,

$$\begin{aligned} \lim_{t \rightarrow b+} I_4(a, b; t) &= C \lim_{t \rightarrow b+} \int_1^b \sqrt{\frac{b-z}{(t-z)(z-1)}} dz = C \int_1^b \sqrt{\frac{1}{z-1}} dz \\ \lim_{t \rightarrow b+} I_5(a, b; t) &= \sqrt{\frac{1}{2b(b^2-1)(b+a)}} \lim_{t \rightarrow b+} \int_b^t \sqrt{\frac{z-b}{t-z}} dz = 0 \\ \lim_{t \rightarrow b+} J_5(a, b; t) &= \sqrt{\frac{a+b}{2b(b^2-1)}} \lim_{t \rightarrow b+} \int_b^t \sqrt{\frac{1}{(t-z)(z-b)}} dz = \pi \sqrt{\frac{a+b}{2b(b^2-1)}} \end{aligned}$$

are also bounded. However

$$\begin{aligned} \lim_{t \rightarrow b+} J_4(a, b; t) &= \lim_{t \rightarrow b+} \int_1^b \frac{1}{\sqrt{(t^2-z^2)(z^2-1)}} \sqrt{\frac{z+a}{b-z}} dz \\ &\geq C \lim_{t \rightarrow b+} \int_1^b \sqrt{\frac{1}{(t-z)(b-z)(z-1)}} dz \\ &\geq C \sqrt{\frac{1}{b-1}} \lim_{t \rightarrow b+} \int_1^b \sqrt{\frac{1}{(t-z)(b-z)}} dz \\ &= 2C \sqrt{\frac{1}{b-1}} \lim_{t \rightarrow b+} \operatorname{arcsinh} \sqrt{\frac{b-1}{t-b}} = \infty \end{aligned}$$

diverges to infinity. Consequently, as $t \rightarrow b+$, we have $Q_I = (I_1 + I_5)/(I_2 + I_4)$ bounded from 0, while $Q_J = (J_1 + J_5)/(J_2 + J_4) \rightarrow 0$, hence $\lim_{t \rightarrow b+} Q > 0$. \square

Now we turn to the limit $t \rightarrow \infty$, which is more amusing.

Proof of (4.2). For the periods in the denominators, we note that

$$\begin{aligned} \lim_{t \rightarrow \infty} t \cdot I_2(a, b; t) &= \int_{-a}^{-1} \sqrt{\frac{1}{z^2-1}} \sqrt{\frac{b-z}{a+z}} dz, \\ \lim_{t \rightarrow \infty} t \cdot J_2(a, b; t) &= \int_{-a}^{-1} \sqrt{\frac{1}{z^2-1}} \sqrt{\frac{a+z}{b-z}} dz, \\ \lim_{t \rightarrow \infty} t \cdot I_4(a, b; t) &= \int_1^b \sqrt{\frac{1}{z^2-1}} \sqrt{\frac{b-z}{a+z}} dz, \\ \lim_{t \rightarrow \infty} t \cdot J_4(a, b; t) &= \int_1^b \sqrt{\frac{1}{z^2-1}} \sqrt{\frac{a+z}{b-z}} dz \end{aligned}$$

are all bounded. We now show that

$$(4.3) \quad \lim_{t \rightarrow \infty} (I_2 + I_4) > \lim_{t \rightarrow \infty} (J_2 + J_4),$$

or equivalently,

$$\lim_{t \rightarrow \infty} (I_2 - J_2) > \lim_{t \rightarrow \infty} (J_4 - I_4).$$

We prove this by considering the functions

$$\begin{aligned} f(a, b) &= \lim_{t \rightarrow \infty} (I_2 - J_2) = \int_1^a \frac{2z - a + b}{\sqrt{(z^2 - 1)(a - z)(b + z)}} dz, \\ g(a, b) &= \lim_{t \rightarrow \infty} (J_4 - I_4) = \int_1^b \frac{2z + a - b}{\sqrt{(z^2 - 1)(a + z)(b - z)}} dz, \end{aligned}$$

and show that $f(a, b) > g(a, b)$ for all $1 < a < b$. Note that $f(a, b) = g(b, a)$. Since

$$\frac{\partial}{\partial b} f(a, b) = \int_1^a \frac{a + b}{\sqrt{(z^2 - 1)(a - z)(b + z)^3}} dz > 0,$$

f is monotone increasing in its second argument for $1 < a < b$. Then g is monotone increasing in its first argument. Note also that $f(a, a) = \pi$ is a constant. Hence

$$f(a, b) > f(a, a) = f(b, b) = g(b, b) > g(a, b),$$

which finishes the proof of (4.3).

The periods in the numerators are more delicate to deal with, as they have logarithmic asymptotics. For instance,

$$\begin{aligned} t \cdot J_5(a, b; t) &= \int_b^t \frac{t}{\sqrt{t^2 - z^2}} \sqrt{\frac{z + a}{z - b}} \sqrt{\frac{1}{z^2 - 1}} dz \\ &> \int_b^t \frac{t}{\sqrt{t^2 - z^2}} \frac{1}{z} dz \\ &= \log \frac{\sqrt{t^2 - b^2} + t}{b}, \end{aligned} \quad (4.4)$$

hence $t \cdot J_5(a, b; t)$ diverges to $+\infty$ as $t \rightarrow \infty$.

Fortunately, the integrals I_1 and J_1 (and I_5 and J_5) have the same logarithmic singularities. By the dominant convergence theorem, we obtain the following estimates:

$$\begin{aligned} \lim_{t \rightarrow \infty} t \cdot (I_1 - J_1) &= \lim_{t \rightarrow \infty} \int_{-t}^{-a} \frac{t(a + b)}{\sqrt{(t^2 - z^2)(z^2 - 1)(b - z)(-a - z)}} dz \\ &= \int_{-\infty}^{-a} \frac{a + b}{\sqrt{z^2 - 1} \sqrt{b - z} \sqrt{-a - z}} dz, \\ \lim_{t \rightarrow \infty} t \cdot (I_5 - J_5) &= \lim_{t \rightarrow \infty} \int_b^t \frac{-t(a + b)}{\sqrt{t^2 - z^2} \sqrt{z^2 - 1} \sqrt{z - b} \sqrt{z + a}} dz \\ &= \int_b^{\infty} \frac{-a - b}{\sqrt{z^2 - 1} \sqrt{z - b} \sqrt{z + a}} dz. \end{aligned} \quad (4.5)$$

Note that they are bounded and non-zero.

Finally, we write

$$Q(a, b; t) = \frac{t(I_1 - J_1) + t(I_5 - J_5)}{tI_2 + tI_4} + t(J_1 + J_5) \left[\frac{1}{tI_2 + tI_4} - \frac{1}{tJ_2 + tJ_4} \right].$$

The part in the square bracket is negative by (4.3). As $t \rightarrow \infty$, the first fraction is bounded by (4.5), and $J_5 \rightarrow +\infty$. This then concludes the proof of the proposition. \square

Before ending this section, we propose the following uniqueness conjecture based on numeric experiments:

Conjecture 4.3. *If $a < b$, then there exists a unique t that solves the period condition (2.3).*

5. INTERSECTION WITH THE MEEKS-LOCUS

By definition, the two families $\text{oD} \subset \mathcal{M}$ and $\text{o}\Delta \subset \mathcal{N}$ are disjoint in \mathcal{D} . However, we will show in this section that the closure $\overline{\text{o}\Delta}$ intersects oD .

To make this precise, we use on \mathcal{D} the topology induced by the space of possible Weierstrass data, which are determined by the four real parameters a, b, t and ρ . Clearly, the convergence of Weierstrass data implies the locally uniform convergence of the minimal surfaces.

The goal is to determine the intersection of the Meeks locus

$$\text{oD} = \{(a, b, t) : Q(a, b; t) = 0, a = b, -t < -a < -1 < 1 < b < t\}$$

with the closure of the non-Meeks locus

$$\text{o}\Delta = \{(a, b, t) : Q(a, b; t) = 0, a \neq b, -t < -a < -1 < 1 < b < t\}.$$

The idea is to divide the function $Q(a, b; t)$ by $b - a$ and take the limit for $a \rightarrow b$ to eliminate solutions in the Meeks locus. We claim:

Theorem 5.1. *The intersection $\overline{\text{o}\Delta} \cap \text{oD}$ is described by the equation*

$$(5.1) \quad \bar{K}(m_1)E(m_2) + \bar{E}(m_1)K(m_2) = \bar{K}(m_1)K(m_2),$$

where

$$K(m) = \int_0^{\pi/2} \frac{1}{\sqrt{1 - m \sin^2(\theta)}} d\theta,$$

$$E(m) = \int_0^{\pi/2} \sqrt{1 - m \sin^2(\theta)} d\theta$$

are complete elliptic integrals of the first and the second kind, $\bar{K}(m) = K(1 - m)$ and $\bar{E}(m) = E(1 - m)$ are the associated elliptic integrals, and the moduli

$$m_1 = \frac{a^2 - 1}{t^2 - 1}, \quad m_2 = \frac{t^2 a^2 - 1}{a^2 t^2 - 1}.$$

Note that $0 < m_1 < m_2 < 1$.

Remark 5.2. It is interesting to notice the similarity of (5.1) with the Legendre relation $\bar{K}(m)E(m) + \bar{E}(m)K(m) - \bar{K}(m)K(m) = \pi/2$.

The theorem follows from the following proposition:

Proposition 5.3. *The function*

$$\tilde{Q}(a, b; t) = \frac{1}{b - a} Q(a, b; t)$$

extends analytically to $a = b$ by

$$\tilde{Q}(a, a; t) = \frac{a(t^2 - 1)}{(a^2 - 1)(t^2 - a^2)} \frac{\bar{K}(m_1)K(m_2) - \bar{K}(m_1)E(m_2) - \bar{E}(m_1)K(m_2)}{K(m_2)^2}.$$

Remark 5.4. Technical details in the following proof are omitted. The integrals we need can all be evaluated in terms of the complete elliptic integrals of the first and the second kind. Integral tables in [BF71] have been very helpful for this purpose, especially after a well-known computer algebra system failed us here.

Proof. We begin by expressing the periods $I_k(a, a; t)$ and $J_k(a, a; t)$ in terms of complete elliptic integrals:

$$I_1(a, a; t) = J_5(a, a; t) = \frac{\bar{K}(m_1) + \bar{K}(m_2)}{\sqrt{t^2 - 1}},$$

$$I_2(a, a; t) = J_4(a, a; t) = \frac{K(m_1) + K(m_2)}{\sqrt{t^2 - 1}},$$

$$I_4(a, a; t) = J_2(a, a; t) = \frac{-K(m_1) + K(m_2)}{\sqrt{t^2 - 1}},$$

$$I_5(a, a; t) = J_1(a, a; t) = \frac{\bar{K}(m_1) - \bar{K}(m_2)}{\sqrt{t^2 - 1}},$$

and combine them into

$$(I_1 + I_5)(a, a; t) = (J_1 + J_5)(a, a; t) = \frac{2\bar{K}(m_1)}{\sqrt{t^2 - 1}},$$

$$(I_2 + I_4)(a, a; t) = (J_2 + J_4)(a, a; t) = \frac{2K(m_2)}{\sqrt{t^2 - 1}}.$$

Then we evaluate the derivatives

$$I'_k(a, a; t) = \frac{\partial}{\partial b} \Big|_{a=b} I_k(a, b, t), \quad J'_k(a, a; t) = \frac{\partial}{\partial b} \Big|_{a=b} J_k(a, b, t),$$

and obtain

$$I'_1(a, a; t) = -I'_5(a, a; t) = \frac{\bar{K}(m_2)}{2a\sqrt{t^2 - 1}}, \quad I'_2(a, a; t) = I'_4(a, a; t) = \frac{K(m_2)}{2a\sqrt{t^2 - 1}},$$

$$J'_1(a, a; t) = -\frac{\bar{K}(m_2)}{2a\sqrt{t^2 - 1}} - \frac{1}{\sqrt{t^2 - 1}} \frac{a}{t^2 - a^2} [-\bar{K}(m_1) + \bar{K}(m_2)] + \frac{\sqrt{t^2 - 1}}{t^2 - a^2} \frac{a}{a^2 - 1} [-\bar{E}(m_1) + \bar{E}(m_2)],$$

$$J'_2(a, a; t) = \frac{K(m_2)}{2a\sqrt{t^2 - 1}} - \frac{1}{\sqrt{t^2 - 1}} \frac{a}{a^2 - 1} [-K(m_1) + K(m_2)] + \frac{\sqrt{t^2 - 1}}{t^2 - a^2} \frac{a}{a^2 - 1} [-E(m_1) + E(m_2)],$$

$$J'_4(a, a; t) = \frac{K(m_2)}{2a\sqrt{t^2 - 1}} - \frac{1}{\sqrt{t^2 - 1}} \frac{a}{a^2 - 1} [K(m_1) + K(m_2)] + \frac{\sqrt{t^2 - 1}}{t^2 - a^2} \frac{a}{a^2 - 1} [E(m_1) + E(m_2)],$$

$$J'_5(a, a; t) = \frac{\bar{K}(m_2)}{2a\sqrt{t^2 - 1}} - \frac{1}{\sqrt{t^2 - 1}} \frac{a}{t^2 - a^2} [-\bar{K}(m_1) - \bar{K}(m_2)] + \frac{\sqrt{t^2 - 1}}{t^2 - a^2} \frac{a}{a^2 - 1} [-\bar{E}(m_1) - \bar{E}(m_2)].$$

They are combined into

$$(I'_2 + I'_4)(a, a; t) = \frac{K(m_2)}{a\sqrt{t^2 - 1}}, \quad (I'_1 + I'_5)(a, a; t) = 0,$$

$$(J'_1 + J'_5)(a, a; t) = \frac{2a\bar{K}(m_1)}{\sqrt{t^2 - 1}(t^2 - a^2)} - \frac{2a\bar{E}(m_1)\sqrt{t^2 - 1}}{(a^2 - 1)(t^2 - a^2)},$$

$$(J'_2 + J'_4)(a, a; t) = \frac{K(m_2)}{a\sqrt{t^2 - 1}} - \frac{2aK(m_2)}{\sqrt{t^2 - 1}(a^2 - 1)} + \frac{2aE(m_2)\sqrt{t^2 - 1}}{(a^2 - 1)(t^2 - a^2)}.$$

Finally, by L'Hospital,

$$\lim_{a \rightarrow b} \frac{1}{b - a} Q(a, b; t) = \frac{\partial Q}{\partial b} \Big|_{a=b} = \frac{a(t^2 - 1)}{(a^2 - 1)(t^2 - a^2)} \frac{\bar{K}(m_1)K(m_2) - \bar{K}(m_1)E(m_2) - \bar{E}(m_1)K(m_2)}{K(m_2)^2}.$$

Now note that the function \tilde{Q} can be extended to a holomorphic function of complex arguments a, b, t . The computation above shows that it remains bounded for $a = b$, and hence extends holomorphically to $a = b$. In particular, the extension for real arguments is real analytic. \square

6. THE TETRAGONAL CASE

We denote by \mathcal{T} surfaces in \mathcal{D} with tetragonal lattice. That is, their unit cells are prisms over squares. We have seen that this occurs when $ab = t$. Again, we have the classical family $t\mathcal{D} = o\mathcal{D} \cap \mathcal{T}$ when $a = b = \sqrt{t}$. The final specialization arises when $t = 2$. In this case, all diagonals and midpoint bisectors of the embedded minimal hexagon are straight lines, and we have the classical D surface.

In this section we will show that $t\Delta = o\Delta \cap \mathcal{T}$ is non-empty and, in fact, a 1-parameter family of surfaces meeting $t\mathcal{D}$ on its boundary.

Lemma 6.1. *For a surface in $t\mathcal{D}$, the period condition is solved if and only if $I_1 + I_5 = I_2 + I_4$.*

Proof. The assumption $t = ab$ implies that $I_k = J_{k+3}$ and $J_k = I_{k+3}$ for $k = 1, 2, 3$. Therefore

$$Q_I = \frac{I_1 + I_5}{I_2 + I_4} = \frac{J_2 + J_4}{J_1 + J_5} = Q_J^{-1}.$$

Hence $Q = Q_I - Q_J = 0$ implies that $Q_I = 1$. \square

We use this lemma to construct right angled hexagons that solve the period problem.

Begin with an axis parallel rectangle R of size $1 \times A$, where $1 < A < 2$ is the height. Draw a line from the top left vertex of R in the 45° south-east direction. Choose a point p on this line in the lower half of R (possible because $A < 2$), and use it as the bottom right vertex of a smaller rectangle R' with the same symmetries. Cut the rectangular annulus between R and R' into four along the symmetry lines. The top right component is a right angled hexagon that solves the period problem.

Its conformal type, however, is still too general. It needs to have a holomorphic involution permuting the edges.

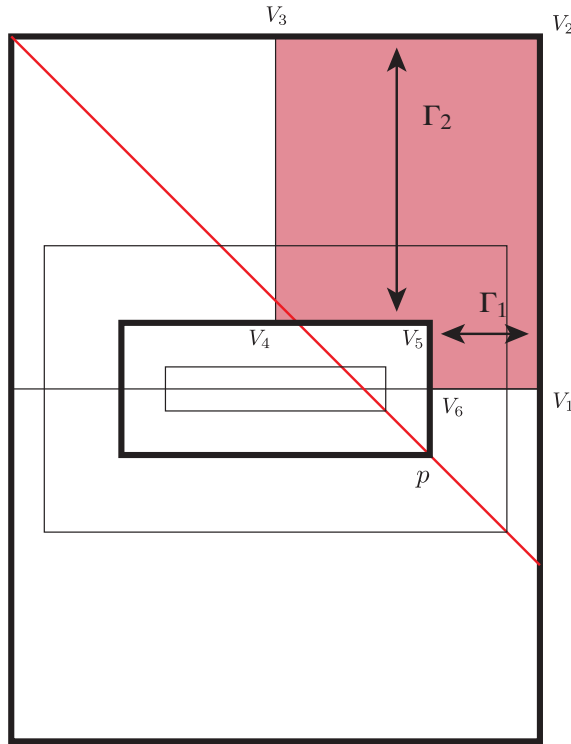


FIGURE 6.1. Existence Proof for $t\Delta$

Theorem 6.2. *For any choice of $1 < A < 2$, there is a choice of p so that the hexagon has a conformal involution.*

Proof. The proof uses an extremal length argument.

Consider the curve families Γ_1 and Γ_2 connecting edges as in Figure 6.1. These families are obtained from each other by the topological order 2 rotation. So in a conformally correct hexagon, they need to have the same extremal length.

Vice versa, we claim that if $\text{ext}\Gamma_1 = \text{ext}\Gamma_2$ then the hexagon has a conformal involution. To see this, we map the hexagon to the upper half plane by the inverse of the Schwarz-Christoffel map $z \mapsto \int^z \phi_1$. The hexagon vertices V_i are mapped to real numbers v_i , and the curve family Γ_1 is mapped to the curves family connecting the edge v_1v_2 with the edge v_5v_6 . Therefore its extremal length is that of the conformal rectangle $v_1v_2v_5v_6$, and thus determines the cross ratio

of these four points. Similarly, the extremal length of Γ_2 determines the cross ratio of the four points $v_2v_3v_4v_5$. If we normalize the v_i as before, the equality of these cross ratios

$$\frac{(a+t)(b+t)}{2t(a+b)} = \frac{(a+1)(b+1)}{2(a+b)}$$

implies that $ab = t$, so the hexagon has indeed a conformal involution.

Thus we have to show that we can adjust the position of p so that the two extremal lengths are equal. Note that moving p to the left will pinch the vertical edge V_5V_6 , while moving p to the right will pinch the horizontal edge V_6V_1 . This shows that the extremal length of Γ_1 will vary between infinity and 0. On the other hand, during this variation, the extremal length of Γ_2 stays bounded away from 0 and infinity. Hence there must be a p for which $\text{ext}\Gamma_1 = \text{ext}\Gamma_2$. \square

Note that the tD family corresponds to the case when both rectangles degenerate to squares.

The intersection of $t\Delta$ with tD can be determined explicitly using the equation from Section 5. Note that for $a = b = \sqrt{t}$, we have

$$m = m_2 = 1 - m_1 = \frac{a^2}{1 + a^2}.$$

Simplifying (5.1) shows that the intersection occurs when

$$2E(m) = K(m).$$

This is solved numerically with $a = a^* = 2.1796604316786983$. We use tD^* to denote the surface with parameter $a = b = \sqrt{t} = a^*$. In Figure 6.2 we compare Schwarz' D surface, the most symmetric surface in the tD family, with the surface tD^* at the junction of tD and $t\Delta$.

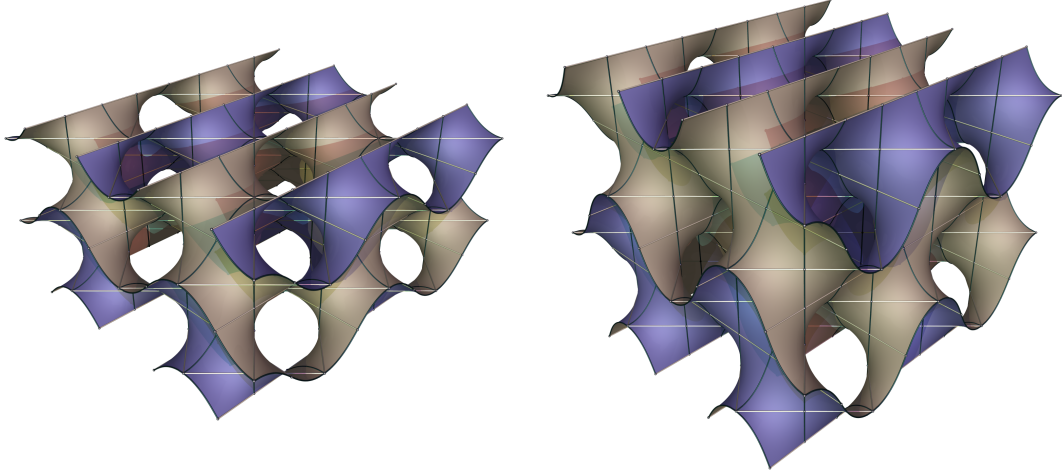


FIGURE 6.2. Schwarz' D and the unstable tD^* surface

In the following, we compare our computation with the bifurcation instances calculated by Koiso, Piccione and Shoda [KPS14]. In particular, there is a pair of conjugate bifurcation instances, one in the tP family and the other in the tD family, for which no bifurcation branch was known. We denote them by tD^+ and tP^+ , respectively.

Since tP^+ was explicitly described in [KPS14], it is easier for us to compare it with the conjugate of tD^* , denote by tP^* . As a surface in the tP family, tP^* can be obtained by rotations from a catenoid spanned by two parallel squares. As in [KPS14], let $E \times E \times F$ be the size of the tetragonal unit cell of tP^* , whose lateral faces are diagonal reflection planes of square catenoids. Using the Weierstrass representation (2.1), we compute that $E/F = 1.05677755 \dots$. This fits perfectly with

the calculation in [KPS14], which gives $E/F = 1.05677757 \dots$ for tP^+ . Consequently, our tD^* surface is exactly the tD^+ surface.

In fact, we also find a bifurcation branch from tP^* , denoted by tII . As one deforms the tetragonal lattice, the horizontal handles deform uniformly along the tP branch. But along the tII branch, the handles in the x direction shrink while the handles in the y direction expand. The tII family turns out to be a subfamily of oPa , a 2-parameter orthorhombic deformation family of Schwarz P surface. Since $\text{oPa} \subset \mathcal{M}$, tII is less interesting for understanding non-Meeks surfaces, hence not a focus of the current paper.

Remark 6.3. Surprisingly, numerical computations show that, near the bifurcation point, $\text{t}\Delta$ surfaces have actually *smaller* area than the corresponding tD surfaces with the same lattice.

REFERENCES

- [BF71] Paul F. Byrd and Morris D. Friedman. *Handbook of elliptic integrals for engineers and scientists*. Die Grundlehren der mathematischen Wissenschaften, Band 67. Springer-Verlag, New York-Heidelberg, 1971. Second edition, revised.
- [Bra92] Kenneth A. Brakke. The surface evolver. *Experiment. Math.*, 1(2):141–165, 1992.
- [Che18] Hao Chen. Minimal twin surfaces. *Exp. Math.*, 2018. online first.
- [ES14] Norio Ejiri and Toshihiro Shoda. On a moduli theory of minimal surfaces. In *Prospects of differential geometry and its related fields*, pages 155–172. World Sci. Publ., Hackensack, NJ, 2014.
- [ES18] Norio Ejiri and Toshihiro Shoda. The Morse index of a triply periodic minimal surface. *Differential Geom. Appl.*, 58:177–201, 2018.
- [FH92] Andrew Fogden and Stephen T. Hyde. Parametrization of triply periodic minimal surfaces. II. regular class solutions. *Acta Cryst. Sect. A*, 48(4):575–591, 1992.
- [FH99] Andrew Fogden and Stephan T. Hyde. Continuous transformations of cubic minimal surfaces. *The European Physical Journal B-Condensed Matter and Complex Systems*, 7(1):91–104, 1999.
- [FHL93] Andrew Fogden, M. Haeberlein, and Sven Lidin. Generalizations of the gyroid surface. *J. Phys. I*, 3(12):2371–2385, 1993.
- [FK89] Werner Fischer and Elke Koch. Genera of minimal balance surfaces. *Acta Cryst. Sect. A*, 45(10):726–732, 1989.
- [KPS14] Miyuki Koiso, Paolo Piccione, and Toshihiro Shoda. On bifurcation and local rigidity of triply periodic minimal surfaces in \mathbb{R}^3 , 2014. preprint, [arXiv:1408.0953](#).
- [LHM01] Hippolyte Lazard-Holly and William H. Meeks, III. Classification of doubly-periodic minimal surfaces of genus zero. *Invent. Math.*, 143(1):1–27, 2001.
- [Mee90] William H. Meeks, III. The theory of triply periodic minimal surfaces. *Indiana Univ. Math. J.*, 39(3):877–936, 1990.
- [MPR98] William H. Meeks, III, Joaquín Pérez, and Antonio Ros. Uniqueness of the Riemann minimal examples. *Invent. Math.*, 133(1):107–132, 1998.
- [MR05] William H. Meeks, III and Harold Rosenberg. The uniqueness of the helicoid. *Ann. of Math. (2)*, 161(2):727–758, 2005.
- [PRT05] Joaquín Pérez, M. Magdalena Rodríguez, and Martin Traizet. The classification of doubly periodic minimal tori with parallel ends. *J. Differential Geom.*, 69(3):523–577, 2005.
- [PT07] Joaquín Pérez and Martin Traizet. The classification of singly periodic minimal surfaces with genus zero and Scherk-type ends. *Trans. Amer. Math. Soc.*, 359(3):965–990, 2007.
- [Sch90] Hermann A. Schwarz. *Gesammelte Mathematische Abhandlungen*, volume 1. Springer, Berlin, 1890.
- [Sch70] Alan H. Schoen. Infinite periodic minimal surfaces without self-intersections. Technical Note D-5541, NASA, Cambridge, Mass., May 1970.
- [Tra08] Martin Traizet. On the genus of triply periodic minimal surfaces. *J. Differential Geom.*, 79(2):243–275, 2008.
- [Wey06] Adam G. Weyhaupt. *New families of embedded triply periodic minimal surfaces of genus three in euclidean space*. ProQuest LLC, Ann Arbor, MI, 2006. Thesis (Ph.D.)–Indiana University.
- [Wey08] Adam G. Weyhaupt. Deformations of the gyroid and Lidinoid minimal surfaces. *Pacific J. Math.*, 235(1):137–171, 2008.

(Chen) GEORG-AUGUST-UNIVERSITÄT GÖTTINGEN, INSTITUT FÜR NUMERISCHE UND ANGEWANDTE MATHEMATIK
E-mail address: h.chen@math.uni-goettingen.de

(Weber) INDIANA UNIVERSITY, DEPARTMENT OF MATHEMATICS
E-mail address: matweber@indiana.edu